IEEE Access
Multidisciplinary | Rapid Review | Open Access Journal

Received September 14, 2020, accepted September 30, 2020, date of publication October 7, 2020, date of current version October 22, 2020.

Digital Object Identifier 10.1109/ACCESS.2020.3029333

Inhomogeneous Image Segmentation Using Hybrid Active Contours Model With Application to Breast Tumor Detection

ASIM NIAZ[1], ASIF AZIZ MEMON[1], KAYNAT RANA[2], (Member, IEEE), ADITI JOSHI[1], SHAFIULLAH SOOMRO[3], JIN SEOK KANG[4], AND KWANG NAM CHOI[1]

[1]Department of Computer Science and Engineering, Chung-Ang University, Seoul 06974, South Korea
[2]Department of Electrical Engineering, University of Engineering and Technology, Taxila 47080, Pakistan
[3]Quaid-e-Awam University of Engineering Science and Technology, Larkana 77150, Pakistan
[4]Department of Biomedical Laboratory Science, Namseoul University, Cheonan 31020, South Korea

Corresponding author: Kwang Nam Choi (knchoi@cau.ac.kr)

This work was supported by the National Research Foundation of Korea (NRF) funded by the Korea Government Ministry of Science and Information Technology (MSIT) under Grant 2019R1F1A1062612.

ABSTRACT The most fatal and frequent cancer amongst women is breast cancer. Mammography provides timely detection of lumps and masses in breast tissue, but effective diagnosis requires accurately identifying malignant tumor boundaries, which remains challenging, particularly for images with inhomogeneous regions. Therefore, we propose an active contour method based on a reformed combined local and global fitted function to address breast tumor segmentation. This combined function is strengthened by a proposed average energy driving function to capture obscure boundaries for regions of interest more precisely from inhomogeneous images. Including a p-Laplace term eliminates reinitialization requirements and suppresses false contours in the segmentation. Bias field signal, which causes image homogeneity corruption, is estimated by bias field initialization to ensure independence from the initial contour position. Local and global fitted models are incorporated by introducing bias fields within them. The proposed method was tested on the MIAS MiniMammographic Database, with quantitative analysis to calculate its accuracy, effectiveness, and efficiency. Experimentation confirmed the proposed method provided superior results compared with previous state-of-the-art methods.

INDEX TERMS Active contours, bias field, image segmentation, intensity inhomogeneity, level set.

I. INTRODUCTION

Breast cancer is the most fatal commonly occurring cancer among women and the second deadliest cancer overall. Early stage detection of breast cancer helps reduce the mortality rate. Mammography is the best tool for early detection of this disease and is used in routine checkups of healthy people. Breast masses are typical breast cancer indicators, and their characteristics reflect tumor growth patterns and biological features. Thus, tumor detection accuracy directly affects breast cancer diagnosis. Complicated breast structure and diverse breast mass features, such shape and geometry, make accurate segmentation difficult. Tumors are subsequently classified as benign or malignant based on their shape regularity.

The associate editor coordinating the review of this manuscript and approving it for publication was Zeev Zalevsky.

Manual breast mass detection is significantly time consuming, with generally reduced detection efficiency due to radiologist's high workload. Various computer aided diagnosis (CAD) systems have been developed to help address manual detection issues, including human error, time, and cost [38]. Medical imaging CAD systems are generally based on image processing and computer vision techniques. Image segmentation is performed to detect tumor cells, classified as regions of interest (ROIs) in mammogram images. Major segmentation challenges within ROIs include the noise, inhomogeneity, and complex weaves. Noise is usually caused by electronic circuitry and/or imaging devices, whereas inhomogeneity arises from object susceptibility to imaging devices and overlaps between intensity ranges within the ROIs.

Several methods have been derived for image segmentation, with various advantages and disadvantages for specific cases, but all with some limitations. The active contour model

(ACM) has been extensively employed to extract smooth segmentation boundaries [1], with the most common ACM image segmentation approaches being edge based: [2]-[5] and region based: [6] - [16]. These segmentation approaches can be applied using active contour techniques depending upon the application. Breast tumor segmentation by ACM is often employed to assist radiologists, since it can readily adjust, grow, and adapt to masses in potentially cancerous areas [17].

Edge based segmentation preserves edges of significant interest defined by a threshold value. Regional local gradient information is utilized to determine active contours, and hence edge based techniques are more effective for images with clear boundaries. Region based segmentation is generally more effective for images with relatively good contrast between foreground and background. The technique is less influenced by mammogram image noise since it generally considers more pixels than edge based methods.

Generally, edge based methods are preferred in terms of algorithm complexity, but region based methods provide better robustness. Region based methods generally assume the ROI comprises homogeneous pixel intensities [4], [7], which makes inhomogeneous image segmentation difficult. A more general piecewise formulation has been proposed [18], [19] to better segment inhomogeneous images, but efficiency is strongly affected by slow computation and sensitivity to contour initialization.

Region based methods include local (LRS) and global (GRS) region segmentation methods. As pointed out in, The Chan– Vese (CV) method [7] uses GRS to segment masses in mammogram images, although local binary fitting (LBF) with LRS can extract accurate local information [6]. LRS methods are generally somewhat superior to GRS methods for inhomogeneous images [7]. However, LRS methods are often favored over GRS methods, they cannot handle all inhomogeneous intensities. Thus, ACMs incorporating multiple object features tend to provide produces better segmentation of mammogram spicules than either LRS or GRS alone [20], [21].

Image inhomogeneity can be estimated by estimating the bias field, and various bias correction methods have been proposed [22] - [27]. The bias field provides the inceptive step for successful segmentation of inhomogeneous images. Zhang *et al.* proposed a local statistical ACM to segment inhomogeneous images, estimating modelling inhomogeneous regions as Gaussian with dissimilar means and variances and then multiplying the original image by the bias field [23], [24]. A local image fitting (LIF) energy functional was defined to limit differences between input image and fitted energy [6], [28], [29]. Li *et al.* proposed a variational level set (VLSBC) approach for simultaneous bias field estimation and image segmentation [22]. The estimated bias field is then subsequently used for image bias correction. The limitation of this method is its dependence on the initial contour, which can affect bias field estimation accuracy. The weighted length regularization (WLR) term suppresses false contours during contour evolution and is independent of re-initialization [30].

This paper proposes a novel hybrid method combining LRS and GRS methods in its energy functional for successful and efficient segmentation of breast masses in digitized mammogram images. The contributions of this research are listed below:

1 Including LRS techniques assists segmentation across inhomogeneous ROIs, whereas GRS accelerates segmentation across homogeneous ROIs.
2 The proposed local average energy function increases overall hybrid method efficiency and facilitates robust contour fitting around potentially cancerous areas.
3 LRS is incorporated with the bias field to improve inhomogeneous ROI segmentation.
4 The WLR term subdues unwanted contour occurrence, providing smoother and more reasonable boundaries.
5 Dependence on initial contour selection was significantly reduced by the new bias field initialization.

The proposed method was tested by segmenting inhomogeneous breast tumors from [32] images, achieving superior detection outcomes for breast masses in mammogram images compared with current state-of-the-art methods. The remainder of this work is organized as follows.

Section II discusses relevant previous studies and Section III describes the proposed methodology. Section IV compares the proposed approach with current best practice methods with respect to time, iterations and different performance metrics. Finally, the section V summarizes and concludes the paper.

II. BACKGROUND WORK

A. CHAN-VESE (CV) METHOD

Suppose $\Omega \subset R^2$ be the image domain and $I : \Omega \rightarrow R^2$ is the given original image. [7] (C-V) proposed an inclusive energy function by dividing the image in to two regions: inside and outside the contour, where both regions assumed to comprise piecewise constant pixel intensities with separable values. Approximate average inner and outer region intensities were classified as g_1 and g_2, respectively. $\phi : \Omega \rightarrow R^2$ is classified as the Lipschitz function representing curve in the CV model. The Lipschitz function is described as a function with bounded first derivative [33]. The zero level set represents contour C, on the image. Thus, the CV model energy minimizing function can be expressed as

$$\begin{aligned} E_{CV}(C, g_1, g_2) &= \lambda_1 \int_\Omega |I(x) - g_1|^2 H_\epsilon(\phi(x))dx \\ &\quad + \lambda_2 \int_\Omega |I(x) - g_2|^2 (1 - H)_\epsilon(\phi(x)))dx \\ &\quad + \mu \int_\Omega |\Delta H_\epsilon(\phi(x))|^2 dx + \nu \int_\Omega H_\epsilon(\phi(x))dx, \end{aligned} \tag{1}$$

where μ,ν and λ_1, λ_2 are scaling constants with values ≥ 0. Contour $C = \{x \in \Omega : \phi(x) = 0\}$, and the average intensities g_1, g_2 are

$$g_1 = \frac{\int_\Omega I(x) H_\epsilon \phi(x))dx}{\int_\Omega H_\epsilon(\phi(x)))} \tag{2}$$

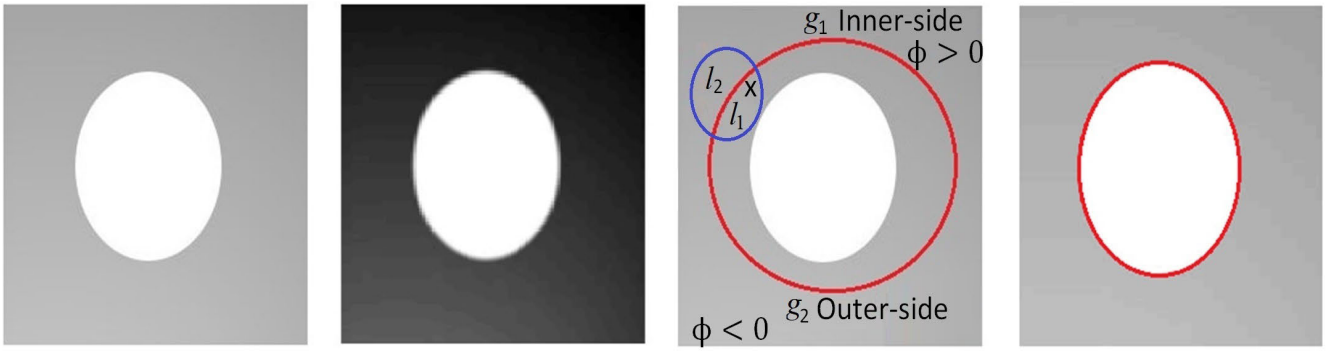

FIGURE 1. Visual representation of the proposed method on an illustrative image: (col 1) input image, (col 2) bias field estimation, (col 3) level set evolution, and (col 4) desired segmentation. Columns 1 and 2 are local and $j1$ and $j2$ are global means. Point x is considered inside the circle locally.

and

$$g_2 = \frac{\int_\Omega I(x)(1 - H_\epsilon\phi(x)))dx}{\int_\Omega (1 - H_\epsilon(\phi(x)))}, \tag{3}$$

where

$$H_\epsilon(\phi(x)) = \frac{1}{2}\left(1 + \frac{2}{\pi} arctan\left(\frac{\phi}{\epsilon}\right)\right) \tag{4}$$

represents the Heaviside function. The derivative of (1) is calculated with respect to ϕ utilizing gradient descent method [34] to provide evolution for the curve, C. The level set function, ϕ, is derived over time for the contour evolution over images. The equivalent level set is expressed as

$$\frac{\partial\phi}{\partial t} = -\lambda_1\delta_\epsilon(\phi)(I - g_1)^2 + \lambda_2\delta_\epsilon(\phi)(I - g_2)^2 + \mu\delta_\epsilon(\phi)div\left(\frac{\Delta\phi}{|\Delta\phi|}\right) - \nu\delta_\epsilon(\phi), \tag{5}$$

where $\delta_\epsilon(\phi)$ is the one-dimensional Dirac delta function,

$$\delta_\epsilon(\phi) = \frac{\epsilon}{\pi(\phi^2 + \epsilon^2)} \tag{6}$$

The width of $\delta_\epsilon(\phi)$ is controlled by parameters in (6). We can regard g_1 and g_2 as object and background intensities since they are global average intensities inside and outside the contour, respectively. Although the CV method is independent of initial contour position, it assumes both intensities are from homogeneous ROIs. Therefore, the method generally fails for inhomogeneous ROIs, producing false segmentation.

B. LOCAL BINARY FITTING (LBF) METHOD

Li *et al.* [29], [6] proposed a local binary fitted (LBF) technique to address image inhomogeneity, utilizing local image information. The proposed LBF model can be expressed as

$$E_{LBF}(C, f_1, f_2) = \lambda_1\int_\Omega K_\sigma(x - y)|I(y) - f_1(x)|^2 H_\epsilon(\phi(y))dy + \lambda_2\int_\Omega K_\sigma(x-y)|I(y)-f_2(x)|^2(1-H_\epsilon(\phi(y)))dy, \tag{7}$$

where λ_1, λ_2 are scaling constants with values ≥ 0, and $H_\epsilon(\phi)$ represents the Heaviside function as explained in (4).

$$f_1(x) = \frac{K_\sigma * [H_\epsilon(\phi)I(x)]}{K_\sigma * H_\epsilon(\phi)} \tag{8}$$

and

$$f_2(x) = \frac{K_\sigma * [(1 - H_\epsilon(\phi))I(x)]}{K_\sigma * (1 - H_\epsilon(\phi))} \tag{9}$$

are local means approximating intensity values inside and outside the contour, respectively. The distance regularization term from [35] is incorporated into (7). The inclusion of distance regularization term guarantee curve evolution stability; and

$$K_\sigma(x - y) = \frac{1}{(2\pi)^{\frac{n}{2}}\sigma^n}\exp^{-\frac{|x-y|^2}{2\sigma^2}} \tag{10}$$

is a Gaussian kernel with scaling parameter σ, i.e., the standard deviation, to balance localization. The energy function from (7) is then minimized with respect to ϕ,

$$\frac{\partial\phi}{\partial t} = -\lambda_1\delta_\epsilon(\phi)\int_\Omega K_\sigma(x - y)|I(x) - f_1(y)|^2 dx + \lambda_2\delta_\epsilon(\phi)\int_\Omega K_\sigma(x - y)|I(x) - f_2(y)|^2 dx + \nu\delta_\epsilon div\left(\frac{\Delta\phi}{|\Delta\phi|}\right) + \mu\left(\Delta\phi - div\left(\frac{\Delta\phi}{|\Delta\phi|}\right)\right), \tag{11}$$

where μ is a constant parameter to initiate curve movement toward object boundaries.

Although the LBF method provides superior results for inhomogeneous image segmentation compared with [7], it still lacks accuracy under some conditions. For example, LBF cannot fully detect the ROI if the initial contour far from the region and contour evolution is stuck in a local minimum.

C. LOCAL IMAGE FITTING (LIF) METHOD

The local image fitted (LIF) method [28] segments inhomogeneous images by introducing LIF energy, i.e., the difference

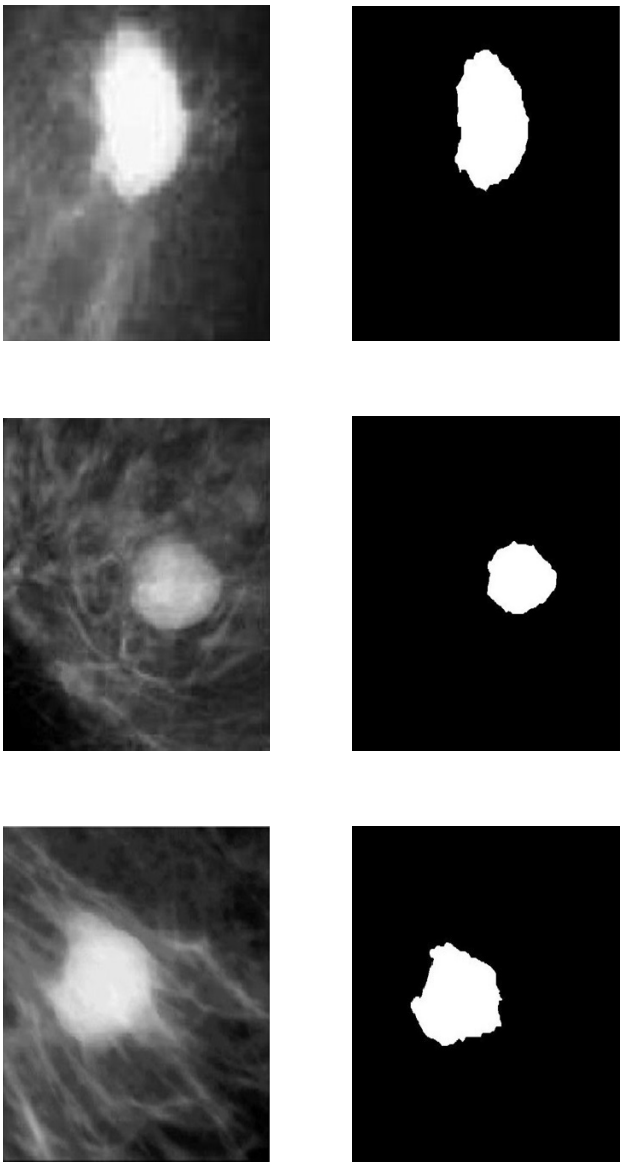

FIGURE 2. Example mini-MIAS database [32] of potential breast cancer (col 1) original images and (col 2) corresponding ground truths.

between fitted and original images,

$$E_{LIF} = \frac{1}{2}\int_{\Omega} |I(x) - I_{LIF}(x)|^2 dx, \tag{12}$$

where I_{LIF} is the locally fitted image,

$$I_{LIF}(x) = f_1(x)H_\epsilon(\phi) + f_2(x)(1 - H_\epsilon(\phi)). \tag{13}$$

where $H_\epsilon(\phi)$ represents the Heaviside function as explained in (4). $f_1(x)$ and $f_2(x)$ are the local means that approximate the intensity values inside and outside the contour, respectively. Minimizing (12) using gradient descent [**?**],

$$\frac{\partial \phi}{\partial t} = (I(x) - I_{LIF}(x))\,(f_1(x) + f_2(x))\,\delta_\epsilon(\phi). \tag{14}$$

This method works well for inhomogeneous images and is computationally less complex than the LBF approach while yielding almost similar segmentation results.

D. VARIATIONAL LEVEL SET WITH BIAS CORRECTION (VLSBC) METHOD

Li *et al.* proposed the variational level set bias correction (VLSBC) model to detect and segment inhomogeneous images [22], [36]. The VLSBC model also provides bias estimation and correction. The model first derives local clustering using a local clustering criterion function to capture neighboring intensities around each point, which is then meshed over the entire domain into a VLSBC formulation. VLSBC defines an image as

$$I(x) = b(x)J(x) + n(x), \tag{15}$$

where $I(x)$) is the original image; $b(x)$ is the bias field, which is assumed to be constantly varying. $J(x)$ is the true image with independent homogeneous regions; and $n(x)$ is additive noise in the image. The local clustering function is based on the iterative procedure of k-means to minimize the energy function,

$$E \approx \int \left(\Sigma_{i=1} \int_{\Omega i}^{N} K_\sigma(x-y)|I(y) - b(x)l_i|^2 dy\right) dx, \tag{16}$$

where c_i represents intensity means for different regions, Ωi represents explicit regions,

$$E = \int \left(\Sigma_{i=1} \int_{\Omega i}^{N} K_\sigma(x-y)|I(y) - b(x)l_i|^2 M_i(\phi) dy\right) dx \tag{17}$$

is the energy functional incorporated with the Heaviside function. (17) $M_i(\phi)$ accounts for the Heaviside function, and its values for the two-phase level set method are

$$M_1(\phi) = H_\epsilon(\phi) \tag{18}$$

and

$$M_2(\phi) = 1 - H_\epsilon(\phi). \tag{19}$$

The true image $J(x)$ from (15) can be mathematically defined as

$$J(x) = \Sigma_{i=1}^{N} l_i M_i(\phi) \tag{20}$$

The mathematical relations for b(x) and li are, derived after taking the first derivative of (17),

$$b(x) = \Sigma_i^N \frac{K_\sigma * (I(x)c_i M_i(\phi))}{K_\sigma * \left(c_i^2 M_i(\phi)\right)}, \tag{21}$$

and

$$l_i = \int \frac{K_\sigma * (I(x)b(x)M_i(\phi))}{K_\sigma * \left(b(x)^2 M_i(\phi)\right)}. \tag{22}$$

The VLSBC method is useful for automatic application due to its robustness to initialization, and it also guarantees bias field smoothness over the data term. However, it has the drawback of dependence on the initial contour position.

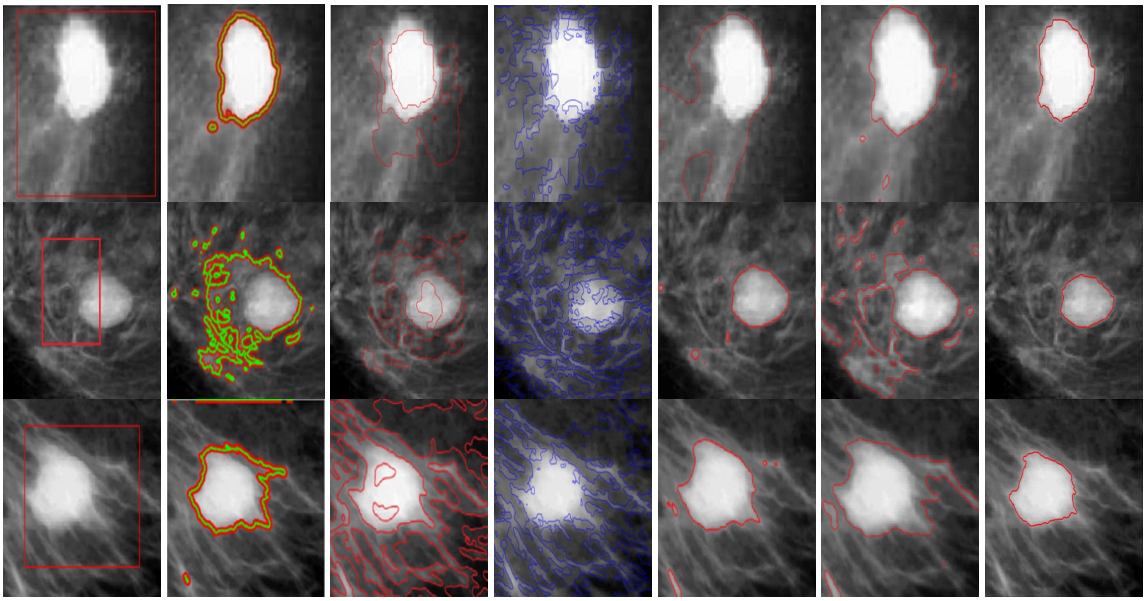

FIGURE 3. Proposed and current best practice methods for the images in Fig. 2: (col 1) input image with initial contour, (col 2) C-V [7], (col 3), LBF [6], (col 4) LIF [28], (col 5) VLSBC [36], (col 6) Zhang *et al.* [24], and (Col 7) proposed method.

E. WEIGHTED LENGTH REGULARIZATION BY P-LaPlace (WLRP) METHOD

Zhou and Mu proposed the weighted length regularization by p-Laplace (WLRP) boundary extraction method [30]. WLRP administers the level set evolution through the p-Laplace equation and the energy function is formed by embedding three other functions,

$$E(\phi) = \lambda_d E_d(\phi) + \lambda_c E_c(\phi) + \lambda_l E_l(\phi), \tag{23}$$

where $E_d(\phi)$ represents the length regularization term as defined for the level set evolution without re-initialization method [35] to stop the level set being too steep or flat; $E_c(\phi)$ is the energy to extract the object; $E_l(\phi)$ is the p- Laplace equation to suppress unnecessary and false contour evolutions. $E_d(\phi)$, $E_c(\phi)$ and $E_l(\phi)$ in (23) are

$$E_d(\phi) = \frac{1}{2}\int_{\Omega}(\Delta\phi - 1)^2 d\Omega, \tag{24}$$

$$E_c(\phi) = \int_{\Omega} H_{\epsilon}(-\phi)|\Delta\phi|^2 d\Omega, \tag{25}$$

and

$$E_l(\phi) = \int_{\Omega} \delta_{\epsilon}(\phi)|\Delta\phi|^p \Omega. \tag{26}$$

$E_d(\phi)$, $E_c(\phi)$ and $E_l(\phi)$ are positive fixed parameters. The WLRP method handles complex topological changes and can eliminate costly re-initialization procedure. Overall, this model offer moderate cost, but cannot segment inhomogeneous images.

F. THE NEW BIAS FIELD INITIALIZATION

The VLSBC bias field initialization is $b(x) = 1$ for $x \in \Omega$ for the zeroth iteration. However, this zero level set may be far from the actual object boundary and hence can lead to inaccurate bias field estimation and consequently inaccurate segmentation.

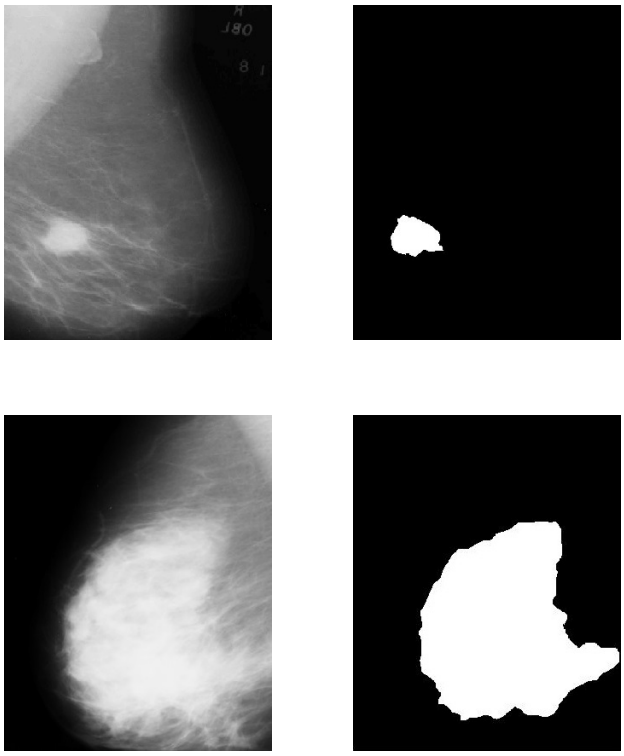

FIGURE 4. Second example mini-MIAS database potential breast cancer (col 1) original images and (col 2) corresponding tumor ground truths.

Huang, Ji, and Zhang introduced a new bias field initialization [31] to overcome the shortcoming. The new bias field initialization assumes that $b(x)$ changes slowly within image

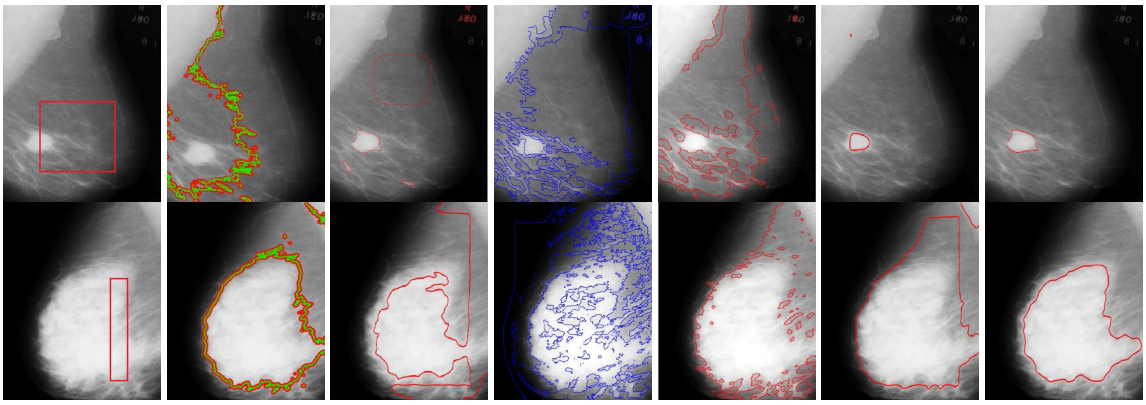

FIGURE 5. Proposed and other state-of-the-art methods for the images from Fig. 4: (col 1) input images with initial contour, (col 2) C-V [7], (col 3), LBF [6], (col 4) LIF [28], (col 5) VLSBC [36], (col 6) Zhang *et al.* [24], and (col 7) proposed method.

domain Ω, hence the new bias field is initialized as

$$b_0 = K_\sigma * \frac{I(x)}{N_0}, \tag{27}$$

where b_0 is the new bias field initialization at the zeroth iteration, and N_0 is the average of image intensities. K_σ stands for the Gaussian kernel and is responsible for the smooth contour evolution. The true image after bias correction, is represented by J_0, can be expressed as

$$J_0 = \frac{I(x)}{b_0} = N_0 \left(\frac{I(x)}{K\sigma * I(x)} \right), \tag{28}$$

which ensures that $N_0 \approx \frac{1}{2}(c_1 + c_2)$ is independent of initial contour position. Thus, b_0 can robustly estimate the bias field.

III. PROPOSED METHODOLOGY

The degree of inhomogeneity in images can be modeled by the VLSBC method (Equation (15),

$$I = b\{l_1 M_1 + l_2 M_2 + \cdots + l_m M_m\}, \tag{29}$$

where b is the modeled true image inhomogeneity classified as a bias field, M_i is the membership function for each region, and l_i is intensity mean calculated for each region independently.

In VLSBC, the bias field estimation depends on initialization because it is initialized as b = 1 and hence can result in incorrect bias field estimation. This limitation is handled by bias field initialization,

$$b_0 = K_\sigma \left(\frac{I}{N_0} \right), \tag{30}$$

where b_0 is the new bias field initialization, K is the Gaussian kernel, and N_0 is the average of image intensities. The bias field is then utilized to formulate the bias corrected image J, if required,

$$J = \frac{I}{b_0}. \tag{31}$$

After the bias field initialization with b_0, it is updated with $b(x)$ from (22) in subsequent iterations. The object boundary

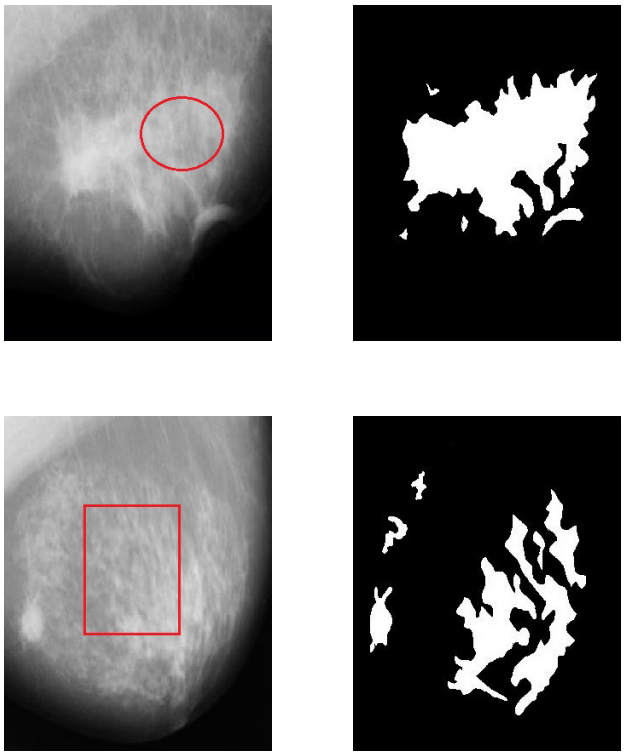

FIGURE 6. Third example mini-MIAS database potential breast cancer (col 1) original images and (col 2) corresponding tumor ground truths.

is an image region with high intensity difference. The new bias field estimation guarantees segmentation independence from the initial contour position [31].

The proposed energy functional for segmenting of intensity-inhomogeneous images is defined as

$$E_{a,LGFI}(\phi) = \alpha E_{LGFI}(\phi) + \mu L_p(\phi) + \nu A(\phi) + E_{LAED}(\phi), \tag{32}$$

where $E_{LGFI}(\phi)$ is a proposed external energy function set incorporating local and global fitted image model advantages, since either approach alone is inadequate for proper

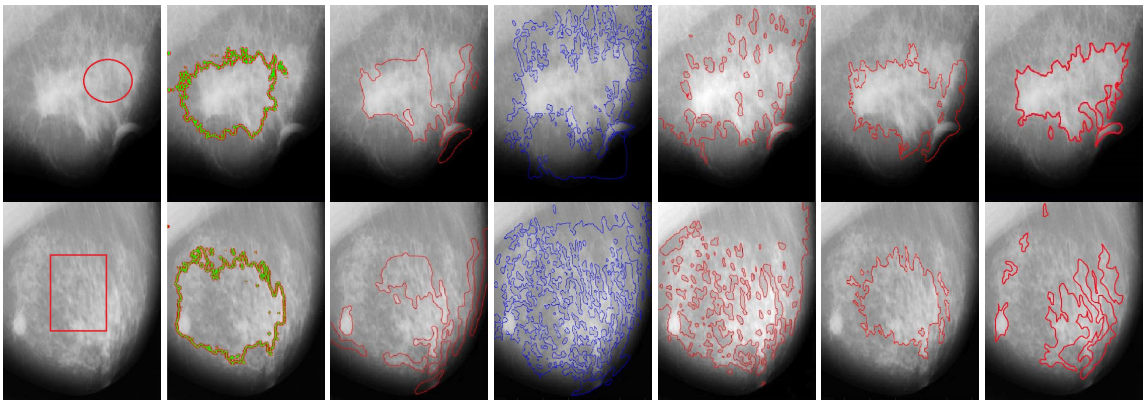

FIGURE 7. Proposed and considered best practice methods for the images from Fig. 6: (col 1) input images with initial contour, (col 2) C-V [7], (col 3), LBF [6], (col 4) LIF [28], (col 5) VLSBC [36], (col 6) Zhang *et al.* [24], and (col 7) proposed method.

inhomogeneous image segmentation. The $E_{LGFI}(\phi)$ model is

$$E_{LGFI}(\phi) = \int w\left((I - I_{bLFI}) + (I - I_{GFI})\right)dx, \tag{33}$$

where

$$I_{bLFI} = (b_0)(l_1M_1 + l_2M_2 + \cdots + l_mM_m) \tag{34}$$

and

$$I_{GFI} = g_1M_1 + g_2M_2 + \cdots + g_mM_m \tag{35}$$

are local and global image fitted models, respectively; g_i and l_i are global and local means as defined in (2), (3) and (22), respectively; M_i represents the membership functions of associated regions and are based on the Heaviside function as per (18) and (19).

where w is the scaling parameter with value ranging from 0 to 1. The value of w is based on the degree of inhomogeneity in the image: larger w implies intensity inhomogeneity in images. In (32) α,μ and v are fixed parameters;

$$L_p(\phi) = \mu \int_{\Omega} \delta_\epsilon(\phi)|\Delta\phi|^p d\Omega \tag{36}$$

is a weighted length regularization term, introduced to eliminate re-initialization and limit false contour evolution [30]; $A(\phi)$ represents the area term, utilized for the speedy curve evolution. The relation to define $A(\phi)$ is as follows:

$$A(\phi) = \int H_\epsilon(\phi) \tag{37}$$

$$E_{LAED}(\phi) = \gamma \int_{\Omega} \delta_\epsilon(\phi)(l_1 + l_2)d\Omega \tag{38}$$

is an externally proposed local average energy driving function, responsible for robust contour fitting and increasing $E_{LGFI}(\phi)$ efficiency.

Global fitted image models are generally designed on the assumption that the input images are homogeneous and the sub regions do not share inhomogeneity. Furthermore, inhomogeneity in Sub regions $\Omega_1, \Omega_2, \ldots, \Omega_n$ could overlap, causing false detection. The proposed method includes local means, which contributes to robustly capturing region inhomogeneity. The local intensity property, combined with the Dirac Delta function, (see (38)) allows effective inhomogeneous image segmentation with improved accuracy and helps to efficiently formulate the bias field.

The scaling parameter, $\gamma = [0, 1]$ depending on image inhomogeneity (see (38)), helps the proposed model to adjust the ROI with improved contour fitting efficiency. We parameterize (32) with respect to time, t, to formulate the level set equation utilizing gradient descent algorithm [**?**],

$$\begin{aligned}\frac{\partial\phi}{\partial t} &= (\alpha)(w)\,(\delta_\epsilon(\phi))\,(b(x))(l_1 + l_2)(I - I_{bLFI}) \\ &\quad + (\alpha)(w)\,(\delta_\epsilon(\phi))\,(g_1 + g_2)(I - I_{GFI}) \\ &\quad + \mu\,(\delta_\epsilon(\phi))\left(div\left(\frac{|\Delta\phi|^p}{|\Delta\phi|^2}\Delta\phi\right)\right) \\ &\quad - v\,(\delta_\epsilon(\phi)) + \gamma(l_1 + l_2)\,(\delta_\epsilon(\phi))\,.\end{aligned} \tag{39}$$

Many iterations, m, are required for efficient breast mass segmentation from inhomogeneous mammogram images and bias field detection, where m differs depending upon convergence. Fig. 1 is a visual representation of the proposed method for an illustrative image.

A. ALGORITHM

The proposed method is summarized as an iterative algorithm as follows.:

IV. RESULTS

he proposed algorithm was implemented and executed in MATLAB® 2018 on Windows 10 installed on a PC with Intel®Core™ i7, 3.60 GHZ and 8192 MB RAM.

The mini-MIAS database [32] included mammograms from 161 different patients. We tested approximately 25% of the available images using the proposed method. The level set method included certain parameters that affect segmentation accuracy and efficiency. We derived near optimal parameter settings by trial and error within indicated ranges extracted from the background work. Table 1 represents the parameters set to generate desired results.

Algorithm 1 Iterative Algorithm for the Proposed Model

Input: The original image $I(x)$, and parameters from Table 1.

1) **Initialize** bias field b_0 following (30)..
2) **Initialize** level set ϕ from $t = 0$,

$$\phi_{t=0} = \begin{cases} -c, & x \in \Omega_0 - \partial\Omega_0 \\ 0, & x \in \partial\Omega_0 \\ c, & x \in \Omega - \partial\Omega_0 \end{cases} \quad (40)$$

where c is constant, Ω represents the image domain with Ω_0 subset, and $\partial\Omega_0$ represents the initial contour boundary.

3) Initialize iteration count, $m = 0$..
4) Calculate local and global intensity means l_1, l_2 and g_1, g_2 from (22) and (2), (3), respectively.
5) Update bias field from (21).
6) Solve potential differential equation in ϕ to obtain $\phi_{(t+1)}$.
7) Check for convergence.

If not, then set $m = m + 1$, repeat steps 4–7.
If converged: final segmented image result is obtained.

TABLE 1. Parameters set to generate desired results.

Parameter	Name	Value
α	Force term	0.999
v	Length term	$0.00001 * 255 * 255$
μ	p-Laplace regularization	1.5
w	Weight	0.999
c	Initial level set	(2)
σ	Gaussian kernel	1.5
Δ	Time step	0.01

For the sake of presentation, three sets of mammogram images form mini-MIAS database are shown in this paper. Fig. 2 shows the first sample of potential breast cancer images with their tumor ground truths generated from information provided in the database [32]. Fig. 3 shows image contour evolution and corresponding segmentation. Table 2 shows the number of iterations and time taken for segmentation to converge. It is clear that our method outclasses the previous methods in terms of processing time and number of iterations taken for contour fitting.

Despite the presence of complex inhomogeneity, the proposed algorithm successfully segmented tumor masses in the breast images; whereas, although the CV method fully covers the ROI (see Fig. 3), it fails to capture accurate boundaries in most cases, and increased processing time and iterations show that the method is inefficient. LIF shows contour evolution in less time than CV, LBF, and Zhang *et al.* methods, and is the second most time efficient (Table 2). However, false contour occurrences highlight the method's weakness. VLSBC and Zhang *et al.* methods achieved good results compared to other current methods, but both had poorer performance than the proposed method. Thus, the proposed method

TABLE 2. Number of iterations and time taken to convergence for methods in Fig. 3.

Methods		Col 1	Col 2	Col 3
CV[7]	CPU Time (s)	12.01	13.24	13.56
	Iterations	500	500	500
LBF [6]	CPU Time (s)	13.45	13.52	12.07
	Iterations	500	500	500
LIF [28]	CPU Time (s)	5.37	5.58	5.42
	Iterations	500	500	500
VLSBC [36]	CPU Time (s)	10.12	9.69	9.45
	Iterations	70	70	70
Zhang et al. [24]	CPU Time (s)	6.29	6.03	7.31
	Iterations	50	50	50
FRAGL [37]	CPU Time (s)	5.69	2.91	2.47
	Iterations	80	31	58
Proposed Model	CPU Time (s)	2.50	2.49	1.69
	Iterations	6	6	6

TABLE 3. Numbers of iterations and time taken to convergence for the methods in Fig. 5.

Methods		Col 1	Col 2
C-V[7]	CPU Time (s)	14.09	13.06
	Iterations	500	500
LBF [6]	CPU Time (s)	14.07	13.71
	Iterations	500	500
LIF [28]	CPU Time (s)	5.67	6.38
	Iterations	500	500
VLSBC [36]	CPU Time (s)	9.87	10.01
	Iterations	50	50
Zhang et al. [24]	CPU Time (s)	6.38	6.89
	Iterations	50	50
FRAGL [37]	CPU Time (s)	4.68	3.82
	Iterations	45	35
Proposed Model	CPU Time (s)	2.67	2.47
	Iterations	6	6

outperformed all considered methods in terms of processing time and number of iterations for convergence.

Fig. 4 shows a second sample set of potential breast cancer images from the mini-MIAS database of mammograms with their respective tumor ground truths. Fig. 5 shows the input images with contour initialization and final results generated by the considered methods, and Table 3 shows the corresponding statistical data for processing time and number of iterations to convergence.

CV could not provide accurate results with inhomogeneity in the image. LBF and LIF also exhibit inaccurate segmentation, due to dependence on the initial contour position. Zhang *et al.* is close to the proposed method in terms of required iterations to convergence, and LIF is close in terms of time efficiency. However, Table 3 confirms that the proposed method successfully segmented breast tumors in less time with greater accuracy compared to all considered state of the art methods.

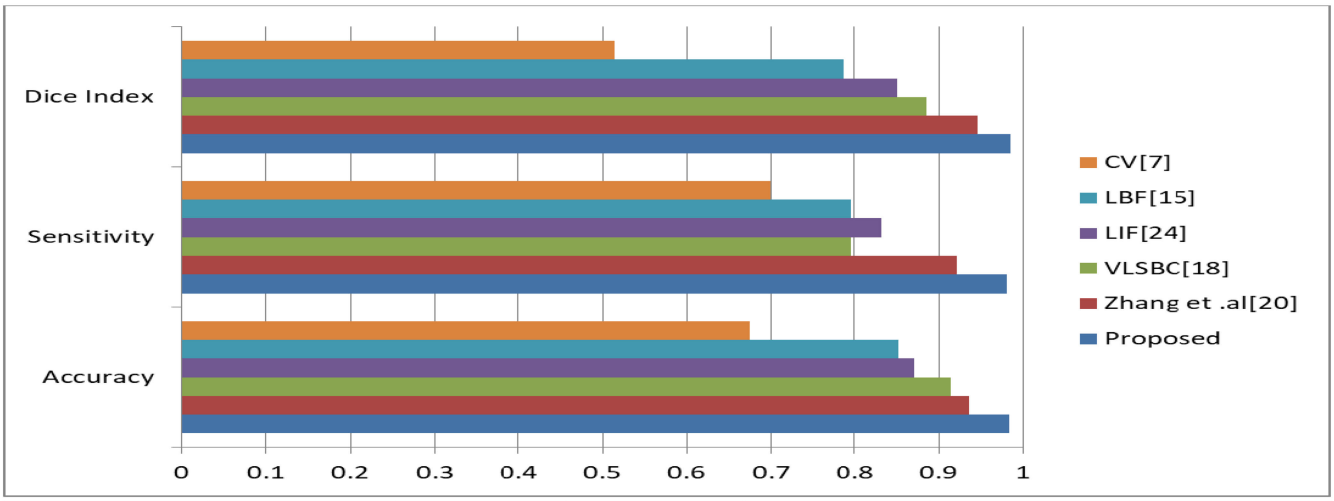

Parameter	CV[7]	LBF[15]	LIF[24]	VLSBC[18]	Zhang et .a[20]	PROPOSED
Accuracy	0.6753	0.8516	0.8716	0.9144	0.9354	0.9839
Sensitivity	0.6989	0.7962	0.8316	0.7965	0.9217	0.9802
Dice Index	0.5138	0.7876	0.8508	0.8856	0.9456	0.9845

FIGURE 8. Performance summary for the considered methods.

TABLE 4. Number of iterations and time taken by each of the method in Figure 7.

Methods		Row 1	Row 2
C-V[7]	CPU Time (s)	13.17	12.67
	Iterations	500	500
LBF [6]	CPU Time (s)	14.67	13.79
	Iterations	500	500
LIF [28]	CPU Time (s)	6.56	6.61
	Iterations	480	480
VLSBC [36]	CPU Time (s)	11.39	10.35
	Iterations	38	26
Zhang et al. [24]	CPU Time (s)	7.42	6.51
	Iterations	50	50
FRAGL [37]	CPU Time (s)	3.96	4.82
	Iterations	22	27
Proposed Model	CPU Time (s)	1.10	2.10
	Iterations	3	4

Fig. 6 shows a third sample set of potential breast cancer images with respective ground truths from the mini-MIAS database; Fig. 7 shows corresponding segregation outcomes from the considered methods, and Table 4 summarizes required number of iterations and CPU time to convergence. The proposed method shows significantly superior performance in terms of segmentation accuracy and CPU time regardless of input image inhomogeneity. However inhomogeneity degrades all considered best practice method segmentation and CPU time requirements.

Figs. 3, 5 and 7 confirm that contour evolution over inhomogeneous mammograms is independent of initial contour

TABLE 5. Mean number of iterations and time taken to convergence for all considered level set methods.

Method	Iterations	Time (Sec)
CV [7]	500	13.01
LBF [6]	500	12.83
LIF [28]	500	05.78
VLSBC [36]	62	09.87
Zhang et .al [24]	50	06.28
FRAGL [37]	44	03.97
Proposed	6	02.41

position for the proposed method, verifying the impact of including the proposed bias field initialization.

Accuracy defines the segmented results closeness to ground truth, whereas sensitivity considers ROI detection, and the Dice index considers ROI overlap with ground truth, defined as

$$Accuracy = \frac{TP + TN}{TP + TN + FP + FN}, \tag{41}$$

$$DiceIndex = \frac{2 \times TP}{2 \times TP + FP + FN}, \tag{42}$$

and

$$Sensitivity = \frac{TP}{TP + FN}, \tag{43}$$

respectively. where TP is the true positive rate, i.e., correctly segmented breast cancer regions; TN is the true negative rate, i.e., correctly unsegmented non-tumor regions; FP is the false positive rate, i.e., non-tumor regions incorrectly categorized as tumors; and FN is the false negative rate, i.e., tumor tissues incorrectly categorized as non-tumor. Fig. 9 compares CPU time to convergence for all considered level set methods.

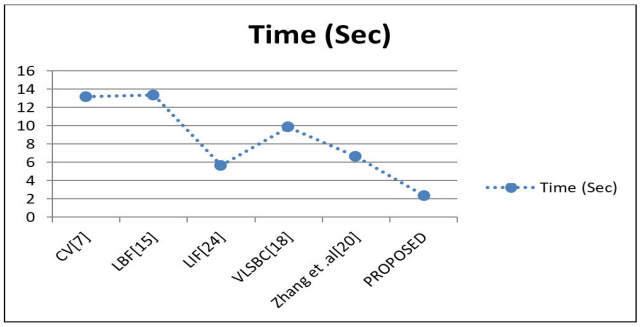

FIGURE 9. **Computational time required for convergence for all the considered methods.**

The obtained results from the quantitative comparisons are considered good if the computed values are near to 1. All obtained matrices through this performance analysis, of all the referenced level set methods confirm the superiority of the proposed hybrid active contour model.

V. CONCLUSION

Accurate breast mass identification is critical for early breast cancer detection. Thus study developed a framework to address intensity inhomogeneity present in mammogram images by combining updated local and global fitted models. We also estimated the bias field to detect image inhomogeneity, and incorporated this contribution in the local fitted function. The updated hybrid function was strengthened by the proposed local average energy driving function to provide effective and efficient contour fitting in malignant mass ROIs for breast images. Computationally expensive re-initialization computations was avoided by adapting the Gaussian filter. Qualitative and quantitative analyses confirmed the proposed method's superior effectiveness, efficiency, and robustness compared with current considered state-of-the-art methods in terms of detecting potential breast cancer regions. Thus, the proposed method offers a powerful tool for early breast cancer detection and consequent mitigation of breast cancer impacts.

CONFLICT OF INTERESTS

The authors declare that there is no conflict of interests regarding the publication of this article.

REFERENCES

[1] M. Kass, A. Witkin, and D. Terzopoulos, "Snakes: Active contour models," *Int. J. Comput. Vis.*, vol. 1, no. 4, pp. 321–331, Jan. 1988.

[2] V. Caselles, R. Kimmel, and G. Sapiro, "Geodesic active contours," *Int. J. Comput. Vis.*, vol. 22, no. 1, pp. 61–79, 1997.

[3] S. Kichenassamy, A. Kumar, P. Olver, A. Tannenbaum, and A. Yezzi, "Gradient flows and geometric active contour models," in *Proc. IEEE Int. Conf. Comput. Vis.*, Jun. 1995, pp. 810–815.

[4] C. Samson, L. Blanc-Feraud, G. Aubert, and J. Zerubia, "A variational model for image classification and restoration," *IEEE Trans. Pattern Anal. Mach. Intell.*, vol. 22, no. 5, pp. 460–472, May 2000.

[5] R. Malladi, J. A. Sethian, and B. C. Vemuri, "Shape modeling with front propagation: A level set approach," *IEEE Trans. Pattern Anal. Mach. Intell.*, vol. 17, no. 2, pp. 158–175, 1995.

[6] C. Li, C.-Y. Kao, J. C. Gore, and Z. Ding, "Minimization of region-scalable fitting energy for image segmentation," *IEEE Trans. Image Process.*, vol. 17, no. 10, pp. 1940–1949, Oct. 2008.

[7] T. F. Chan and L. A. Vese, "Active contours without edges," *IEEE Trans. Image Process.*, vol. 10, no. 2, pp. 266–277, 2001.

[8] R. Ronfard, "Region-based strategies for active contour models," *Int. J. Comput. Vis.*, vol. 13, no. 2, pp. 229–251, Oct. 1994.

[9] S. Soomro, A. Munir, and K. N. Choi, "Hybrid two-stage active contour method with region and edge information for intensity inhomogeneous image segmentation," *PLoS ONE*, vol. 13, no. 1, Jan. 2018, Art. no. e0191827.

[10] P. P. Rebouças Filho, P. C. Cortez, A. C. D. S. Barros, and V. H. C. de Albuquerque, "Novel adaptive balloon active contour method based on internal force for image segmentation—A systematic evaluation on synthetic and real images," *Expert Syst. Appl.*, vol. 41, no. 17, pp. 7707–7721, Dec. 2014.

[11] M. Ciecholewski, "An edge-based active contour model using an inflation/deflation force with a damping coefficient," *Expert Syst. Appl.*, vol. 44, pp. 22–36, Feb. 2016.

[12] A. Vard, A. Monadjemi, K. Jamshidi, and N. Movahhedinia, "Fast texture energy based image segmentation using directional Walsh–Hadamard transform and parametric active contour models," *Expert Syst. Appl.*, vol. 38, no. 9, pp. 11722–11729, Sep. 2011.

[13] G. Liu, H. Li, and L. Yang, "A topology preserving method of evolving contours based on sparsity constraint for object segmentation," *IEEE Access*, vol. 5, pp. 19971–19982, 2017.

[14] S. Zhu, X. Bu, and Q. Zhou, "A novel edge preserving active contour model using guided filter and harmonic surface function for infrared image segmentation," *IEEE Access*, vol. 6, pp. 5493–5510, 2018.

[15] A. Munir, S. Soomro, C. H. Lee, and K. N. Choi, "Adaptive active contours based on variable kernel with constant initialisation," *IET Image Process.*, vol. 12, no. 7, pp. 1117–1123, Jul. 2018.

[16] S. Soomro, F. Akram, A. Munir, C. H. Lee, and K. N. Choi, "Segmentation of left and right ventricles in cardiac MRI using active contours," *Comput. Math. Methods Med.*, vol. 2017, pp. 1–16, 2017.

[17] G. S. Muralidhar, A. C. Bovik, J. D. Giese, M. P. Sampat, G. J. Whitman, T. M. Haygood, T. W. Stephens, and M. K. Markey, "Snakules: A model-based active contour algorithm for the annotation of spicules on mammography," *IEEE Trans. Med. Imag.*, vol. 29, no. 10, pp. 1768–1780, Oct. 2010.

[18] A. Tsai, A. Yezzi, and A. S. Willsky, "Curve evolution implementation of the mumford-shah functional for image segmentation, denoising, interpolation, and magnification," *IEEE Trans. Image Process.*, vol. 10, no. 8, pp. 1169–1186, Aug. 2001.

[19] L. A. Vese and T. F. Chan, "A multiphase level set framework for image segmentation using the Mumford and Shah model," *Int. J. Comput. Vis.*, vol. 50, no. 3, pp. 271–293, Dec. 2002.

[20] S. Ali and A. Madabhushi, "An integrated region-, boundary-, shape-based active contour for multiple object overlap resolution in histological imagery," *IEEE Trans. Med. Imag.*, vol. 31, no. 7, pp. 1448–1460, Jul. 2012.

[21] S. Soomro, A. Munir, and K. N. Choi, "Fuzzy c-means clustering based active contour model driven by edge scaled region information," *Expert Syst. Appl.*, vol. 120, pp. 387–396, Apr. 2019.

[22] C. Li, R. Huang, Z. Ding, J. C. Gatenby, D. N. Metaxas, and J. C. Gore, "A level set method for image segmentation in the presence of intensity inhomogeneities with application to MRI," *IEEE Trans. Image Process.*, vol. 20, no. 7, pp. 2007–2016, Jul. 2011.

[23] K. Zhang, Q. Liu, H. Song, and X. Li, "A variational approach to simultaneous image segmentation and bias correction," *IEEE Trans. Cybern.*, vol. 45, no. 8, pp. 1426–1437, Aug. 2015.

[24] K. Zhang, L. Zhang, K.-M. Lam, and D. Zhang, "A level set approach to image segmentation with intensity inhomogeneity," *IEEE Trans. Cybern.*, vol. 46, no. 2, pp. 546–557, Feb. 2016.

[25] C. Li, J. C. Gore, and C. Davatzikos, "Multiplicative intrinsic component optimization (MICO) for MRI bias field estimation and tissue segmentation," *Magn. Reson. Imag.*, vol. 32, no. 7, pp. 913–923, Sep. 2014.

[26] L. Wang, J. Zhu, M. Sheng, A. Cribb, S. Zhu, and J. Pu, "Simultaneous segmentation and bias field estimation using local fitted images," *Pattern Recognit.*, vol. 74, pp. 145–155, Feb. 2018.

[27] B. Johnston, M. S. Atkins, B. Mackiewich, and M. Anderson, "Segmentation of multiple sclerosis lesions in intensity corrected multispectral MRI," *IEEE Trans. Med. Imag.*, vol. 15, no. 2, pp. 154–169, Apr. 1996.

[28] K. Zhang, H. Song, and L. Zhang, "Active contours driven by local image fitting energy," *Pattern Recognit.*, vol. 43, no. 4, pp. 1199–1206, Apr. 2010.
[29] C. Li, C.-Y. Kao, J. C. Gore, and Z. Ding, "Implicit active contours driven by local binary fitting energy," in *Proc. IEEE Conf. Comput. Vis. Pattern Recognit.*, Jun. 2007, pp. 1–7.
[30] B. Zhou and C.-L. Mu, "Level set evolution for boundary extraction based on a p-Laplace equation," *Appl. Math. Model.*, vol. 34, no. 12, pp. 3910–3916, Dec. 2010.
[31] G. Huang, H. Ji, and W. Zhang, "A fast level set method for inhomogeneous image segmentation with adaptive scale parameter," *Magn. Reson. Imag.*, vol. 52, pp. 33–45, Oct. 2018.
[32] *The Mini-Mias Database of Mammograms*.
[33] I. Marx and G. Piranian, "Lipschitz functions of continuous functions," *Pacific J. Math.*, vol. 3, no. 2, pp. 447–459, Jun. 1953.
[34] G. Aubert and P. Kornprobst, *Mathematical Problems in Image Processing: Partial Differential Equations and the Calculus of Variations*, vol. 147. Cham, Switzerland: Springer, 2006.
[35] C. Li, C. Xu, C. Gui, and M. D. Fox, "Level set evolution without re-initialization: A new variational formulation," in *Proc. IEEE Comput. Soc. Conf. Comput. Vis. Pattern Recognit. (CVPR)*, vol. 1, Jun. 2005, pp. 430–436.
[36] C. Li, R. Huang, Z. Ding, C. Gatenby, D. Metaxas, and J. Gore, "A variational level set approach to segmentation and bias correction of images with intensity inhomogeneity," in *Proc. Int. Conf. Med. Image Comput. Comput.-Assist. Intervent.* Cham, Switzerland: Springer, 2008, pp. 1083–1091.
[37] J. Fang, H. Liu, L. Zhang, J. Liu, and H. Liu, "Fuzzy region-based active contours driven by weighting global and local fitting energy," *IEEE Access*, vol. 7, pp. 184518–184536, 2019.
[38] K. Doi, "Computer-aided diagnosis in medical imaging: Historical review, current status and future potential," *Computerized Med. Imag. Graph.*, vol. 31, nos. 4–5, pp. 198–211, Jun. 2007.

ASIM NIAZ received the B.S. degree in electrical (computer) engineering from the COMSATS Institute of Information Technology, Pakistan, in 2016. He is currently pursuing the M.S. degree with the Department of Computer Science and Engineering, Chung-Ang University, Seoul, South Korea.

Since 2018, he has been working as a Research Assistant with the Visual Image Media Laboratory, Chung-Ang University, under Prof. Dr. Choi. He is also a Graduate Research Student with the Department of Computer Science and Engineering, Chung-Ang University. His current research interests include medical image analysis, semantic segmentation, and generative modeling.

ASIF AZIZ MEMON received the B.E. and M.E. degrees from Mehran UET, Jamshoro, Pakistan, in 2010 and 2015, respectively. He is currently pursuing the Ph.D. degree in application software with Chung-Ang University, Seoul, South Korea.

Since 2018, he has been working as a Research Assistant with the Visual Image Media Laboratory, Chung-Ang University, under Prof. Dr. Choi. His research interests include image segmentation, image recognition, and medical imaging.

KAYNAT RANA (Member, IEEE) received the B.S. degree in electrical (computer) engineering from the COMSATS Institute of Information Technology, Pakistan, in 2016. She is currently pursuing the M.S. degree with the Department of Electrical Engineering, University of Engineering and Technology, Taxila, Pakistan.

Since 2017, she has been working as a Lab Engineer (Junior Lecturer) with the Department of Computer Science and Engineering, HITEC University, Taxila. Her current research interests include medical image analysis, electronics, and generative modeling.

ADITI JOSHI received the B.S. degree in computer science and the M.B.A. degree in marketing from Mumbai University, India, in 2014 and 2016, respectively. She is currently pursuing the M.S. degree with the Department of Computer Science and Engineering, Chung-Ang University, Seoul, South Korea.

Since 2019, she has been working as a Research Assistant with the Visual Image Media Laboratory, Chung-Ang University, under Prof. Dr. Choi. Her current research interests include medical image analysis, semantic segmentation, and face and gesture recognition.

SHAFIULLAH SOOMRO received the B.E. degree from the Quaid-e-Awam University of Engineering, Science and Technology (QUEST), Nawabshah, Pakistan, in 2008, the M.E. degree from MUET, Jamshoro, Pakistan, in 2014, and the Ph.D. degree in computer science from Chung-Ang University, Seoul, South Korea, in 2018.

He is currently an Assistant Professor of computer science with QUEST, Larkana, Pakistan. His research interests include motion tracking, object segmentation, and 3-D image recognition.

JIN SEOK KANG received the Doctor of Veterinary Medicine (DVM) and M.S. degrees from Seoul National University, South Korea, in 1990 and 1992, respectively, and the Ph.D. degree in medicine from Osaka City University, Japan, in 2006.

He is currently a Professor with the Department of Biomedical Laboratory Science, Namseoul University, Cheonan, South Korea. His current research interest includes pathology.

KWANG NAM CHOI received the B.S. and M.S. degrees from the Department of Computer Science, Chung-Ang University, Seoul, South Korea, in 1988 and 1990, respectively, and the Ph.D. degree in computer science from the University of York, U.K., in 2002.

He is currently a Professor with the School of Computer Science and Engineering, Chung-Ang University. His current research interests include motion tracking, object categorization, and 3D image recognition.